PARTICIPANT INTIMACY
A cluster analysis of the intranuclear cascade†

J. CUGNON*

Kellogg Radiation Laboratory, California Institute of Technology, Pasadena, California 91125, USA

and

J. KNOLL** and J. RANDRUP

Nuclear Science Division, Lawrence Berkeley Laboratory, Berkeley, California 94720, USA

Received 25 September 1980

Abstract: The intranuclear cascade for relativistic nuclear collisions is analyzed in terms of "clusters" consisting of groups of nucleons which are dynamically linked to each other by violent interactions. The formation cross sections for the different cluster types as well as their intrinsic dynamics are studied and compared with the predictions of the linear cascade model ("rows-on-rows").

1. Introduction

The first-generation experiments with relativistic nuclear beams (with energies of 0.2–2 GeV per nucleon) have concentrated on the observation of a single reaction product. The gross features of these one-particle inclusive spectra can be fairly well reproduced by a number of models based on widely different physical assumptions. Recently, considerable progress has been made towards obtaining more detailed information. Current measurements of coincidence spectra and one-particle spectra with associated multiplicities of other ejectiles call for more detailed models and may yield better insight into the detailed collision dynamics††.

At the present, no complete and still tractable theory of high-energy nuclear collisions exists. The most detailed description is provided by the intra-nuclear cascade model [2,3]). (INC) It follows the fate of the individual nucleons (and any additional particles produced) as they suffer multiple collisions governed by our knowledge of the elementary two-particle dynamics. Calculations within this model are rather cumbersome and the results are often intransparent: all the different effects – be they of geometrical, kinematical or dynamical origin – are interwoven and difficult to disentangle. In fact, the complexity of the calculated results are comparable to that of the experimental data. This makes it so much more necessary

† This work was supported in part by the US Department of Energy under Contract W-7405-ENG-48, and by the US National Science Foundation Grant PHY76-83685, and the German Heisenberg Stiftung.

* Present address: Physics Department, University of Liège, B-4000 Sart/Tilman, Liège 1, Belgium.

** Heisenberg Fellow, Present address: GSI, Postfach 110541, D-6100, Darmstadt, W. Germany.

†† The most recent review of the field can be found in ref. [1]).

to try to understand the collisions in terms of simple models based on well-defined idealizations. [Well-known examples of such simplistic models are the knock-out [4]), the fireball [5]), the firestreak [6]), and the statistical [7]) models.] On the other hand, the wealth of information produced in an intra-nuclear cascade calculation allows us to ask questions about dynamical details which are experimentally beyond reach but which may be essential for our understanding of the collision process.

A relatively successful, but still transparent, multiple collision model is the linear cascade model, the so-called "rows-on-rows" model [8]). A detailed analysis of high-energy nucleon collisions has been made in ref. [9]). The major advantage of the linear cascade model is the separation of *geometrical* and *dynamical* aspects: the initial geometry of the nuclei essentially determines which groups of nucleons will interact violently among each other while the dynamics of these interactions is solely reflected in the corresponding spectral shapes. It is the aim of the present study to test these simple models against a *full-scale* intra-nuclear cascade calculation which treats the space-time evolution of the multiple collision process in detail. The goal is to express the cascade result in terms similar to those used in the simplified approaches, by studying the common fate of those nucleons which have had intimate dynamical encounters during the collision process.

2. Intimacy – the cluster decomposition

The starting point for our discussion is the observation that any multiple-collision process can be subjected to a cluster decomposition. Two particles are classified as belonging to the same cluster if they have had at least one violent interaction in the course of the collision process. (The precise meaning of "violent" will be given later.) It then follows that particles belonging to different clusters have at most interacted gently with each other. By use of this concept the complicated collision diagram for the entire process can be decomposed into a number of sub-processes, each involving considerably fewer particles; the different clusters can, to a first approximation, be treated as dynamically independent but the relatively weak mutual interaction could be included perturbatively. In this way, in close analogy to the simple models, the discussion of the collision process structures into two separate parts: one is concerned with the relative probability for the occurrence of the different types of clusters and the other deals with the intrinsic dynamics of a given cluster type.

In our present study we are interested only in clusters which contain at least one nucleon from each of the two colliding nuclei, A and B. These clusters are named the *participants*, the remaining ones being *spectators*. We shall characterize a given cluster by its number of projectile nucleons and target nucleons (m_k, n_k) so that the cluster decomposition of a given collision event can be characterized by

$$\underset{\sim}{c} = \{m_1 n_1, m_2 n_2, \ldots, m_c n_c\},$$

where c is the total number of (participant) clusters. The total number of participant nucleons is

$$\nu = \nu_A + \nu_B = \sum_{i=1}^{c} m_i + \sum_{j=1}^{c} n_j ,$$

and their final momenta are denoted by $\boldsymbol{p}_1, \ldots, \boldsymbol{p}_\nu$. The cross section for producing such an event represents the most exclusive quantity available for our study[†],

$$\sigma_{AB}(\varsigma; \boldsymbol{p}_1 \cdots \boldsymbol{p}_\nu) . \tag{1}$$

Less exclusive information can be obtained from these cross sections by defining the following inclusive cross section[‡]

$$\langle \mathcal{Q}(\varsigma; \boldsymbol{p}_1 \cdots \boldsymbol{p}_\nu) \rangle_{AB} \sigma^r_{AB} = \sum_{\varsigma} \int \frac{d\boldsymbol{p}_1}{E_1} \cdots \int \frac{d\boldsymbol{p}_\nu}{E_\nu} \mathcal{Q}(\varsigma; p_1 \cdots p_\nu) \sigma_{AB}(\varsigma; \boldsymbol{p}_1 \cdots \boldsymbol{p}_\nu) . \tag{2}$$

Here $\mathcal{Q}$ specifies the type of inclusive observable considered and σ^r_{AB} is the total reaction cross section as obtained by putting $\mathcal{Q}$ equal to unity;

$$\sigma^r_{AB} = \sum_{\varsigma} \int \frac{d\boldsymbol{p}_1}{E_1} \cdots \int \frac{d\boldsymbol{p}_\nu}{E_\nu} \sigma_{AB}(\varsigma; \boldsymbol{p}_1 \cdots \boldsymbol{p}_\nu) . \tag{3}$$

Thus the detection of only one particle at given momentum $\boldsymbol{p}$ and energy E results in the one-particle inclusive spectrum,

$$E \frac{d\sigma}{d\boldsymbol{p}} \equiv \sigma_{AB}(\boldsymbol{p}) = \sigma^r_{AB} \left\langle \sum_{k=1}^{\nu} E \delta(\boldsymbol{p} - \boldsymbol{p}_k) \right\rangle_{AB} , \tag{4}$$

which is simply related to the mean (participant) multiplicity $\langle \nu \rangle$

$$\int \frac{d\boldsymbol{p}}{E} \sigma_{AB}(\boldsymbol{p}) = \sigma^r_{AB} \langle \nu \rangle . \tag{5}$$

The major advantage of the cluster decomposition is that all one-particle observables, such as the inclusive spectrum or the mean multiplicity, are given simply in terms of the corresponding mutually independent contributions from the different cluster types,

$$\sigma_{AB}(\boldsymbol{p}) = \sum_{MN} \sigma_{AB}(M, N; \boldsymbol{p}) = \sum_{MN} \sigma_{AB}(M, N) F_{ABMN}(\boldsymbol{p}) , \tag{6a}$$

$$\langle \nu \rangle \sigma^r_{AB} = \sum_{MN} (M + N) \sigma_{AB}(M, N) . \tag{6b}$$

[†] We attempt to keep the notation such that arguments in parentheses refer to the observables, whereas subscripts such as AB or MN specify the auxiliary conditions.

[‡] Which in a quantum mechanical scheme amounts to calculating the trace Tr $\mathcal{Q}\rho$, where ρ is the many-body density matrix.

This feature naturally suggests two key quantities for the subsequent discussion. One is the partial cross section for forming a given type of cluster, formally defined as

$$\sigma_{AB}(M,N)=\sigma^{r}_{AB}\left\langle \sum_{k=1}^{c}\delta(M-m_k)\delta(N-n_k)\right\rangle_{AB}. \tag{7}$$

The other is the spectral distribution of the nucleons of a given cluster type,

$$F_{ABMN}(\boldsymbol{p})=\sigma_{AB}(M,N,\boldsymbol{p})/\sigma_{AB}(M,N), \tag{8}$$

where

$$\sigma_{AB}(M,N,\boldsymbol{p})=\sigma^{r}_{AB}\left\langle \sum_{k=1}^{c}\delta(M-m_k)\delta(N-n_k)\sum_{i=1}^{m_k+n_k}E\delta(\boldsymbol{p}-\boldsymbol{p}_i)\right\rangle_{AB}. \tag{9}$$

The normalization of the spectral functions is

$$\int\frac{d\boldsymbol{p}}{E}F_{ABMN}(\boldsymbol{p})=M+N. \tag{10}$$

It readily follows that the mean number of clusters generated in the nucleus–nucleus collision is given by

$$\langle c\rangle\sigma^{r}_{AB}=\sum_{MN}\sigma_{AB}(M,N), \tag{11}$$

so that in turn the mean cluster size is

$$\langle M+N\rangle=\frac{\langle\nu\rangle}{\langle c\rangle}=\frac{\Sigma(M+N)\sigma_{AB}(M,N)}{\Sigma\sigma_{AB}(M,N)}. \tag{12}$$

The essential building blocks for the one-particle observables in the complex collision are the cluster formation cross sections (7) and the cluster spectra (8). The general cluster expansion of the inclusive cross section (6) is recognized in many of the simple collision models. Most of these infer the formation cross sections from simple geometrical considerations (often using straight line trajectories) but adopt widely different dynamical pictures to construct the spectra F.

The questions we seek to answer in the following are: How do these key quantities look when calculated in a full-scale multiple collision model? and how do they compare with simpler, idealized pictures?

3. Intra-nuclear cascade versus simplicity

In this section we briefly recall the main ingredients of the INC model employed† and of the rows-on-rows model. Detailed descriptions are given in ref. [3,9]), respectively.

† Not all cascade models are suitable for a cluster analysis since some of them describe one of the nuclei as a continuous medium rather than a collection of nucleons.

Throughout the violent phase of the reaction only nucleons and their delta isobars are considered whereas pions are created only after this phase through the free decay of the remaining deltas. Initially, the nucleons of both nuclei occupy sharp-sphere spatial distributions with radii of $R = r_0 A^{1/3}$ ($r_0 = 1.12$ fm) and a sharp-sphere momentum distribution (Fermi distribution) with a Fermi momentum of $P_F = 270$ MeV/c. The binary collision cross sections are generalized from known NN data by detailed balance and other arguments to the unmeasured processes (e.g., $N\Delta \to \Delta\Delta$). While the INC traces the particles in three dimensions between two subsequent interactions, the rows-on-rows model adopts a simple straight-line picture: All nucleons which are initially situated in a beam oriented tube of transverse extension of the total NN cross section, σ_{NN}^{tot} (≈ 40 mb), form a cluster. The cluster formation cross sections $\sigma_{AB}(M, N)$ are then simply related to the initial spatial geometry of the two nuclei. The intrinsic cluster dynamics is determined by demanding that the M projectile nucleons interact sequentially with all the N target nucleons, changing their momenta and baryonic state (N or Δ) in each binary collision.

Although the INC interweaves geometry with dynamics it is still possible to discuss these aspects separately.

4. Geometrical aspects

The sharp-sphere nuclear densities employed lead to a total reaction cross section given by

$$\sigma_{AB}^{r} \approx \pi (R_A + R_B)^2 ,$$

or slightly less since the finite mean free path makes the nuclear edges partially transparent. The next quantity most closely related to geometry is the mean participant multiplicity. Straight-line geometry yields [8])

$$\langle \nu \rangle_{AB} \sigma_{AB}^{r} = A\sigma_B^{r} + B\sigma_A^{r} ,$$

where $\sigma_A^{r} \approx \pi R_A^2$ and $\sigma_B^{r} \approx \pi R_B^2$ are the respective nucleon–nucleus reaction cross sections. Thus, for equal-mass systems one would have $\sigma_{AB}^{r} \approx 4\sigma_A^{r}$, and hence $\langle \nu \rangle \approx \frac{1}{2}A$ which agrees well with the INC results

$$\langle \nu \rangle_{NeNe} = 10.7 , \qquad \langle \nu \rangle_{CaCa} = 23 .$$

In addition to these more obvious integral geometrical properties we also expect the cluster formation cross sections to be closely related to geometry. For this purpose, however, we first have to specify more precisely the terms "gentle" and "violent" interactions.

4.1. GENTLE OR VIOLENT

A given binary collision is classified as "gentle" if the following two criteria are satisfied:

(i) The collision is elastic (i.e., $NN \to NN$, $N\Delta \to N\Delta$, or $\Delta\Delta \to \Delta\Delta$).

(ii) The four-momentum transfer is less than a certain cut-off value: $|t| < q_c^2$. Here $t = (E_i' - E_i)^2 - (\boldsymbol{p}_i' - \boldsymbol{p}_i)^2 c^2$ for a collision between particles i and j[†].

With the above criteria it is elementary to analyze the history of each nucleus–nucleus collision and obtain the cluster formation cross sections $\sigma_{AB}(M, N)$. A simple illustration of such a cluster decomposition is shown in fig. 1.

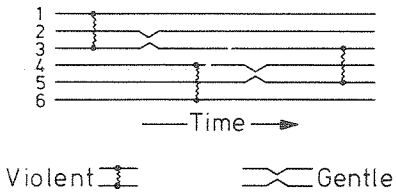

Fig. 1. The decomposition of a six-particle collision into the clusters (1, 3, 5), (4, 6) and (2).

Intra-nuclear cascade calculations have been analyzed for various values of the cut-off parameter q_c. In the extreme limit of vanishing cut-off (i.e., *all* interactions are classified as violent), rather large clusters result, with sizes up to the total number of participants. Many of these large clusters consist of subclusters which are only linked to each other by a few rather gentle collisions. They therefore quickly break apart as q_c is increased. The cluster formation cross sections are consequently quite sensitive to q_c but, as we shall see later, the intrinsic dynamics of a given cluster type is not.

Fig. 2 shows the dependence of the average cluster size $\langle M+N\rangle_{AB}$ as a function of the cut-off parameter q_c. As expected, $\langle M+N\rangle$ drops off with increasing q_c, but in a slightly more drastic way for the heavier system. For Ne+Ne the cluster sizes for central ($b = 0$) and peripheral ($b = 1.87R$) collisions are also shown. The peripherally produced clusters contain only around two nucleons corresponding to a single knock-out process (or none for large q_c), while those arising in the central collisions are quite large. The latter are seen to shrink in a more drastic way with increasing q_c than for peripheral clusters.

A physically reasonable scale for the cut-off parameter q_c is provided by the initial Fermi motion. Hence we have chosen a standard value of

$$q_c = P_F = 270\ \mathrm{MeV}/c\,.$$

The mean cluster size estimated by straight-line geometry are $\langle M+N\rangle = 4.9$ and 6.1, respectively, which are substantially lower than those calculated with $q_c = 270\ \mathrm{MeV}/c$ (see fig. 2).

The above choice, $q_c = P_F$, implies that the fluctuation in each cluster's mean momentum $\langle \boldsymbol{P}\rangle_{MN}$ due to the gentle collisions is of about the same order or less than that due to the intrinsic Fermi motion. These gentle interactions represent a residual "friction" force between the clusters which tends to reduce their relative mean

[†] This criterion assumes that the labels of the final identical particles $(i', j') = (i, j)$ or (j, i) have been chosen so as to give the least value of $|t|$.

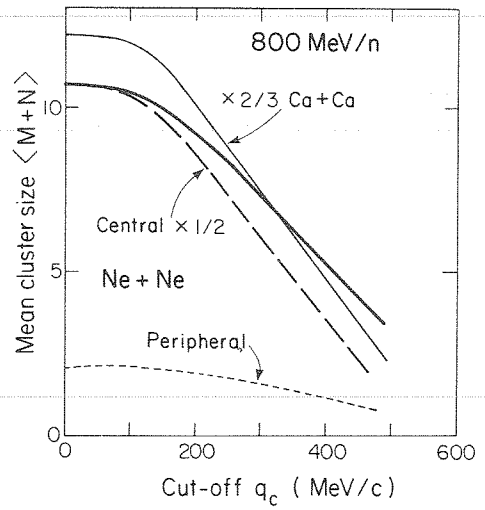

Fig. 2. The mean cluster size $\langle M+N\rangle$ as a function of the cut off q_c. For Ne+Ne: the long-dashed curve is the result for central collisions ($b=0$) and the short-dashed curve corresponds to peripheral collisions ($b=1.87R$); the over-all average for all impact parameters is indicated by the heavy full curve. The light full curve shows the over-all average for Ca+Ca, multiplied by $\frac{2}{3}$ for convenience.

velocity. To gain insight into the transport of energy and momentum between the different clusters one may study the incurred dispersions in the cluster momenta, i.e., calculate for each cluster type the mean square deviation between the final momentum

$$\boldsymbol{P}' = \sum_{k=1}^{M+N} \boldsymbol{P}'_k ,$$

per particle from that given initially

$$\boldsymbol{P} = \sum_{k=1}^{M+N} \boldsymbol{P}_k ,$$

$$(\Delta P_{\parallel}^2)_{MN} = \frac{1}{(M+N)^2}\langle (P'_{\parallel} - P_{\parallel})^2\rangle ,$$

$$(\Delta P_{\perp}^2)_{MN} = \frac{1}{(M+N)^2}\langle (P'_{\perp} - P_{\perp})^2\rangle .$$

(Note that $\perp$ refers to an arbitrary transverse direction so that $\langle P_{\perp}^2\rangle = \langle P_x^2\rangle = \langle P_y^2\rangle$ while $P_{\parallel} = P_z$.) These dispersions arise solely from the gentle interactions with other clusters. The transverse dispersion reflects the statistical nature of the momentum exchange between the clusters while the longitudinal momentum dispersion also contains the contribution from the average shift in the cluster momentum.

The above momentum dispersions are displayed in fig. 3 in the form of kinetic energies per nucleon. These energies, typically a few or several MeV are quite small

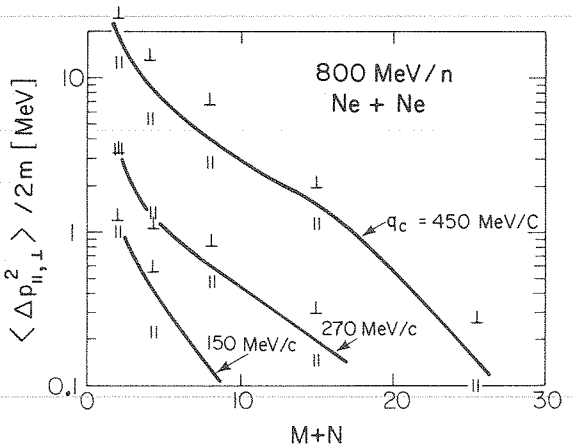

Fig. 3. The dispersions in the cluster momenta as functions of the cluster size $M+N$, for three different values of the cut off q_c. The symbol $\parallel$ refers to the momentum component parallel to the beam and $\perp$ refers to the transverse component. The lines are drawn to guide the eye to the results belonging to the same q_c.

in comparison with typical kinetic energies in the system which are given by $\frac{1}{2}\tau \approx 40$ MeV for each translational degree of freedom. The cluster decomposition is therefore meaningful and residual cluster interactions can be neglected without any noticeable effect on the observable spectra. We note that the transverse dispersions are larger than the longitudinal ones. This is a consequence of the forward-peaked nature of the gentle collisions which makes the defect in momentum transfer preferentially perpendicular to the direction of motion.

The dependence of the cluster structure on the impact parameter b is illustrated in more detail in fig. 4 for Ne + Ne and Ca + Ca. The circles indicate the mean number of participants, $\langle \nu \rangle_b$, divided by the total number of nucleons, $2A$. The two results are

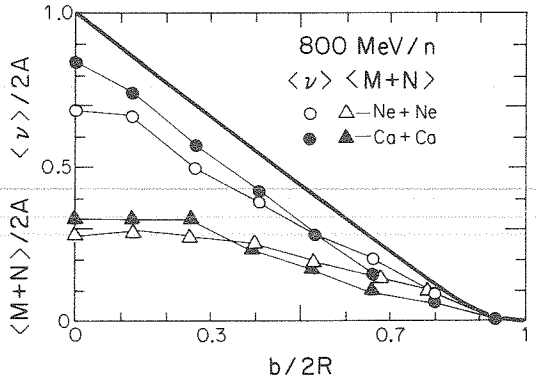

Fig. 4. The mean cluster size $\langle M+N \rangle$ (triangles) and the mean number of participants $\langle \nu \rangle$ (circles) as functions of the impact parameter b. The open symbols are for Ne + Ne and the solid symbols are for Ca + Ca. The full line indicates the universal curve for $\langle \nu \rangle$ resulting from the clean cut of two equal sharp-sphere matter distributions.

nearly identical but both somewhat below the sharp-sphere overlap estimate, due to the partial transparency. The triangles show the mean cluster sizes (also divided by $2A$). Again, the two results are nearly identical, suggesting an approximate scaling with the total nucleon number. The figure also indicates that central collision events contain about three clusters on the mean while there is at most one cluster for a peripheral impact.

4.2. THE FORMATION CROSS SECTIONS

The previous discussion concentrated on mean values. More detailed insight can be gained from the behavior of the formation cross sections themselves. As their dependence on M and N as obtained from the INS is not suitable for a contour plot, two projections will be discussed:

(i) The dependence on the total cluster size $M+N$:

$$\sigma_{AB}(M+N) = (M+N) \sum_{M'+N'=M+N} \sigma_{AB}(M', N') .$$

(ii) The dependence on the mass asymmetry $\eta(M, N) = M/(M+N)$:

$$\sigma_{AB}(\eta)\Delta\eta = \sum_{\eta(M,N)\in\eta\pm\Delta\eta/2} (M+N)\sigma_{AB}(M, N) .$$

This mass ratio, as already considered in the fire-streak model [6]), is the quantity relevant for the over-all kinematics of each cluster. It specifies its available c.m. energy and its mean momentum. The above two projections are displayed in fig. 5 for the case of Ne+Ne; the results for Ca+Ca are quite similar, except for an over-all scaling.

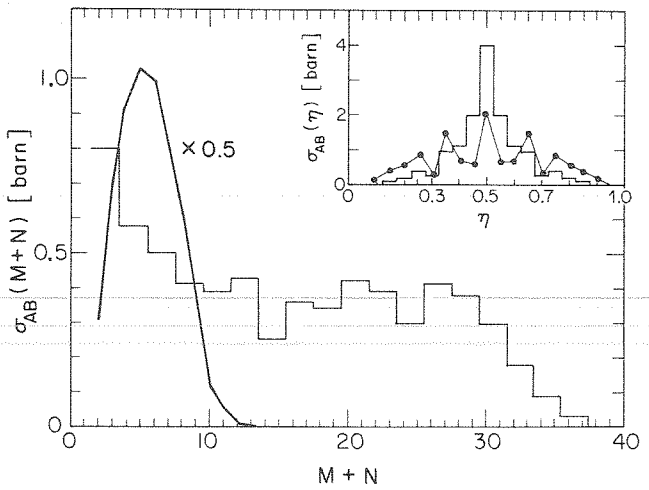

Fig. 5. The cross sections for observing a nucleon arising from a given cluster size $M+N$, as calculated for 800 MeV/n Ne+Ne (histogram); the kinked curve is the rows-on-rows result. The insert shows the cross sections for observing a nucleon resulting from a cluster with a given mean velocity (characterized by the asymmetry parameter $\eta = M/(M+N)$); the same notation is used.

As for the dependence on the cluster size, we note a striking dissimilarity: in the rows-on-rows picture there is no transverse communication and the cluster sizes depend only on the local thickness of the nuclei. This picture strongly inhibits the formation of large clusters and the ensuing distribution is peaked at the relatively small value of $\langle M+N\rangle \approx 6$. Although the dynamics predominantly evolves in the longitudinal direction there is some transverse communication. As we shall see later, already the finite range of the NN force will tend to link neighboring clusters. It should be noted, though, that the so produced large clusters would have a structure of two or several subclusters joined by only one or a few dynamical links. Therefore, their internal dynamical state may still resemble that corresponding to smaller clusters. The actual analysis of the respective spectra will in fact support this conjecture (see below).

Though it is very important to study the shapes of the spectra F_{MN} characteristic of the various clusters (sect. 5), it is of equal importance to know how the different spectra add up to the final one-particle spectrum. As already mentioned this is dominantly governed by the mass asymmetry parameter η. The centroids of each spectrum $F_{MN}(\boldsymbol{p})$ are placed simply at

$$\langle P\rangle_{MN} = \eta P_{\mathrm{A}} + (1-\eta) P_{\mathrm{B}} ,$$

where P_{A} and P_{B} are the momenta per nucleon of the two nuclei. Thus, even if all the cluster spectra F_{MN} were isotropic, the dispersion in η produces an elongation of the inclusive one-particle spectrum. The top part of fig. 5 indicates that the linear collision model produces dispersions $(\Delta\eta)^2$ which are about twice the INC values. Again this deviation can be understood on the basis of the relatively large clusters in the cascade calculation.

4.3. TRANSVERSE COMMUNICATION

One of the main advantages of the intra-nuclear cascade model is that it provides detailed information of the spatial evolution of the collision process. In high-energy nuclear collisions the dynamics is predominantly forward directed and several models build on the idealization that no communication occurs in the transverse direction. To elucidate the transverse dynamics we study the following quantity

$$\langle s^2\rangle_{MN} = \frac{1}{M+N}\sum_{k=1}^{M+N} s_k^2 - \left(\frac{1}{M+N}\sum_{k=1}^{M+N} s_k\right)^2 ,$$

which expresses the dispersion in the initial transverse positions of the nucleons in a given cluster type. It thus provides a measure of how far in the transverse direction a given nucleon can influence the dynamics. In fig. 5 $\langle s^2\rangle$ is shown as a function of the cluster size $M+N$. The results show an initial linear increase with cluster size, nearly identical for the two systems considered, followed by a gradual leveling off towards system-dependent limiting values.

It is easy to understand these features. The entire process can be thought of as a problem of throwing discs randomly on the floor, where each disc has a cross section $\frac{1}{4}\sigma_{NN}^{tot}$. The value for $M = N = 1$ is then the average dispersion in separation for those pairs of discs which happen to overlap and is therefore given by $\langle s^2 \rangle_{11} = \sigma_{NN}^{tot}/2\pi$. The clusters are made up of those discs which cover a connected area. The growth in dispersion with cluster size is then a diffusion process characterized by a diffusion coefficient $D = \sigma_{NN}^{tot}/4\pi$. The initial rate of growth is therefore $d\langle s^2 \rangle_{MN}/d(M+N) = 2D = \sigma_{NN}^{tot}/2\pi = \langle s^2 \rangle_{11}$, in good agreement with the calculated results. The fact that the nucleons are confined inside the nuclei corresponds to having a bounded floor (walls). The dispersions then gradually saturate and approach a value reflecting the transverse extension of the system. The total nucleon–nucleon cross section σ_{NN}^{tot} is more or less constant over a wide range of energy and the boundary of the "floor" remains fixed (in other words the total reaction cross section is a constant). Hence, we expected the cluster decomposition to be fairly independent of the incident kinetic energy per particle in the GeV range. At lower energy, the amount of transverse communication is probably maintained by the compensating effects of a smaller nucleon–nucleon cross section σ_{NN}^{tot} and of a more isotropic angular distribution. So, we believe that our results concerning the cluster decomposition are qualitatively valid down to, say 250 MeV/A incident kinetic energy.

The over-all good agreement of the INC results with the above picture suggests that the transverse communication predominantly arises from the *finite* extension of the nucleons (as expressed through σ_{NN}^{tot}) rather than from actual transverse motion. It would be possible to incorporate this effect into the straight-line picture and thus, among other things, obtain a simple tool for predicting the substructure of the large clusters.

5. Cluster dynamics

We have discussed above various aspects of the cluster formation. We now turn to the question of the internal structure of the clusters, i.e., how their total energy and momentum is shared among the constituents.

Fig. 7 displays some quantities characterizing the momentum distribution of the nucleons, as a function of the cluster size. The upper portion is the momentum dispersions in the longitudinal and transverse directions. We observe a large similarity between clusters produced in Ne + Ne and Ca + Ca collisions. This finding supports the universality of the cluster dynamics and hence the usefulness of the cluster analysis. The degree of kinematic equilibrium attained within a given cluster type can be characterized by the isotropy parameter $I = (\langle p_\perp^2 \rangle / \langle p_\parallel^2 \rangle)^{1/2}$. The values of $\langle p_\parallel^2 \rangle^{1/2}$ and $\langle p_\perp^2 \rangle^{1/2}$ are shown in fig. 6 together with their ratio I. The INC results for I are typically around 0.8 indicating a slight preference for motion along the beam direction. The linear cascade results exhibit a faster relaxation towards isotropy, followed by a gradual decrease of I due to the particular collision sequence

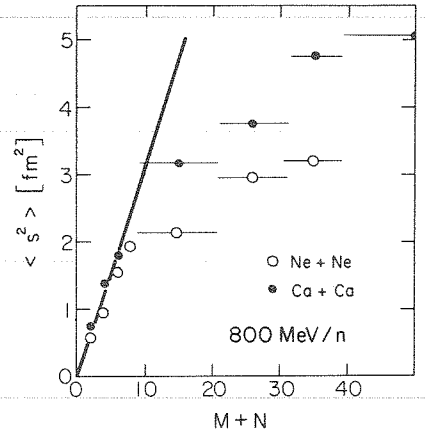

Fig. 6. The dispersion in the initial transverse positions s_k of the nucleons belonging to the same cluster of a given size $M+N$. The straight line is the result for the disc-throwing analogy discussed in the text.

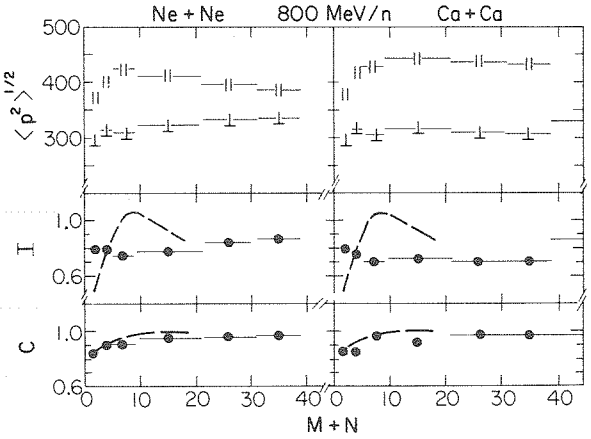

Fig. 7. The upper portion shows the longitudinal ($\|$) and transverse ($\perp$) widths of the nucleon spectra for different cluster sizes $M+N$. The corresponding isotropy parameter $I = \langle p_\perp \rangle^{1/2} / \langle p_\| \rangle^{1/2}$ is shown in the middle portion while the lower portion shows the crookedness $\frac{3}{5}\langle p^4 \rangle / \langle p^2 \rangle^2$ of the spectral profile. When present, the horizontal bars indicate averaging over a range of cluster sizes.

imposed in the linear cascade. These findings are fairly independent of the cut-off chosen, except for the knock-out component $M = N = 1$. For finite values of q_c the most forward scattering events will be classified as gentle and the isotropy parameter will be increased (since the elementary NN cross section is forward peaked). When q_c is reduced to zero these events are included and the isotropy drops from 0.80 to 0.61 in accordance with the rows-on-rows results.

Another quantity characterizing the cluster spectra is the crookedness of the momentum profile. We adopt the parameter $C = \frac{3}{5}\langle p^4 \rangle / \langle p^2 \rangle^2$ which is unity for a

maxwellian distribution. This quantity relaxes quickly towards unity as a function of cluster size and follows closely the linear-cascade result.

In nucleon–nucleon collisions at 800 MeV/N there is an appreciable chance ($\approx 50\%$) of converting one of the baryons into a delta resonance. This introduces additional complexity into the collision dynamics. The results presented above are for the final nucleon spectra, i.e., after the deltas have eventually converted back into nucleons by pion emission. Fig. 8 shows the relative number of deltas present in the various cluster types at the end of the violent collision stage. From a value of around 0.20–0.25 for small clusters (reflecting the branching ratio in NN collisions) there is a decrease towards a value of around 0.12, which is somewhat lower than the Boltzmann value of 0.16. A similar behavior was already found in the rows-on-rows model [9]).

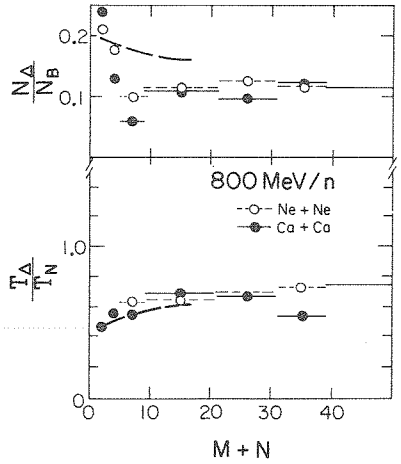

Fig. 8. Upper portion: the relative number of baryons in the delta state as a function of the cluster size $M+N$. Lower portion: the mean kinetic energy of a Δ-particle relative to that of a nucleon. On both portions the dashed curves indicate the rows-on-rows results. When present, the horizontal bars indicate averaging over a range of cluster sizes.

The degree of kinetic equilibrium attained can be elucidated by the ratio T_Δ/T_N between the kinetic energies carried by the two kinds of baryons. At 800 MeV/N the deltas are produced with a relatively low kinetic energy (the threshold is at 600 MeV/N). By additional collisions the deltas gradually acquire more kinetic energy but the equilibrium value $T_\Delta \approx T_N$ is never reached.

Altogether the spectra calculated by the intranuclear cascade follow quite closely the results obtained in the simple rows-on-rows dynamics. The spectra shapes do not change any more beyond a cluster size of 10 nucleons. The anisotropy of about 80% persisting up to very big clusters may indicate that these consist of subclusters of more equilibrated structure linked together by only one or a few interactions. This aspect could be clarified in a future study analyzing the substructure of the clusters.

6. Conclusion

In the study presented we have made an attempt to disentangle the apparently complicated results of an intranuclear cascade calculation in analyzing its basic building blocks: its clusters, comprising those nucleons which were in intimate interaction contact. In this way we achieved a formulation of the collision problem close to those used in simplified approaches, then making possible direct comparisons with simple physical ideas.

When making the cluster decomposition it is necessary to distinguish between gentle and violent interactions. This was done by means of a cut off in momentum transfer. We found that the cut off chosen was of no significant dynamical relevance.

The main results are:

(i) Given a specific cluster size, the resulting nucleon spectrum does not depend much on the colliding nuclei A and B (universality).

(ii) The spectral shapes are found to be in close agreement with those calculated with the simple rows-on-rows prescription. Beyond a cluster size of about 8 nucleons the shape of these spectra do not change any more, indicating that a kind of bulk limit is attained.

The greatest discrepancy with simplified models appears in the size of the clusters formed. While the straight-line concept in the rows-on-rows model leads to fairly small clusters, the intranuclear cascade links many nucleons into the same clusters. The main reason for these large sizes produced in the INC was traced to the finite value in the NN interaction radius which leads to an increase in transverse communication as the size of the cluster grows. Still, a structural analysis of these large clusters would probably reveal them as built up of several subclusters linked by only one or two interactions. Hence the subclusters may reflect more directly the dynamics of the process.

We see the presented analysis as an aid to reducing the inherent complexity of the intranuclear cascade description. In particular, the cluster decomposition may improve the practical utility of the INC for the study of relatively rare events, such as high-momentum components or multi-particle coincidences.

We have benefitted from discussions with S. Bohrmann, M. Gyulassy and S.E. Koonin. One of us (J.C.) wishes to thank the Kellogg Radiation Laboratory for its hospitality. Another of us (J.K.) is grateful to the Heisenberg Stiftung for its support and to the Nuclear Theory Group at Lawrence Berkeley Laboratory for its hospitality.

References

1) Proc. INS-Kikuchi Summer School on nuclear physics at high energies, Fuji-Yoshida, Japan, July 1–4, 1980

2) J.P. Bondorf, H.T. Feldmeier, S. Garpman and E.C. Halbert, Phys. Lett. **65B** (1976) 217; Z. Phys. **279** (1976) 385;

R.K. Smith and M. Danos, unpublished
K.K. Gudima and V.D. Toneev, Yad. Fiz. **27** (1978) 658 [Sov. J. Nucl. Phys. **27** (1978) 351];
K.K. Gudima, H. Iew and V.D. Toneev, J. of Phys. **G5** (1978) 229;
J.D. Stevenson, Phys. Rev. Lett. **41** (1978) 1702;
Y. Yariv and Z. Fraenkel, Phys. Rev. **C20** (1979) 2227; and to be published;
E.C. Halbert, Density patterns and energy-angle distributions from a simple cascade scheme for fast Ne + U collisions, ORNL preprint (1980);
C.C. Noack, preprint, University of Bremen, Germany
3) J. Cugnon, Phys. Rev. **C22** (1980) 1885;
J. Cugnon, T. Mizutani and J. Vandermeulen, Nucl. Phys. **A352** (1981) 505;
J. Cugnon and S.E. Koonin, to be published
4) S.E. Koonin, Phys. Rev. Lett. **39** (1977) 680;
R.L. Hatch and S.E. Koonin, Phys. Lett. **81B** (1979) 1
5) J. Gosset, H.H. Gutbrod, W.G. Meyer, A.M. Poskanzer, A. Sandoval, R. Stock and G.D. Westfall, Phys. Rev. **C16** (1977) 629
6) W.D. Myers, Nucl. Phys. **A296** (1978) 177;
J. Gosset, J.I. Kapusta and G.D. Westfall, Phys. Rev. **C18** (1978) 844
7) J. Knoll, Phys. Rev. **C20** (1979) 773; Nucl. Phys. **A343** (1980) 511;
S. Bohrmann and J. Knoll, LBL-10970 (1980)
8) J. Hüfner and J. Knoll, Nucl. Phys. **A290** (1977) 460;
J. Randrup, Nucl. Phys. **A316** (1979) 509
9) J. Knoll and J. Randrup, Nucl. Phys. **A324** (1979) 445